Validation of Virtual Life Management® with Ti-6Al-4V Test Data for Smooth and Notched Specimens

Robert G. Tryon and Animesh Dey
VEXTEC Corporation

ABSTRACT

This paper proposes a probabilistic analysis framework incorporating material fatigue response models at the microstructural scale to predict the scatter in damage behavior for an ensemble of test specimen. The material fatigue response model uses micromechanical fatigue analysis to properly account for the multiple stages of early fatigue damage that drives the scatter in fatigue response. Observations from the open literature are used to determine fatigue damage accumulation mechanisms at the microstructural level for an *α-β* Ti-6Al-4V alloy. The fatigue stages of crack nucleation, small crack growth and long crack growth are explicitly considered. Theoretical and semi-empirical models that relate the damage to the fatigue response are developed for each stage. The statistics of the microstructural variables that govern the scatter in the fatigue response are estimated. A Monte Carlo Simulation algorithm is developed to combine the three stages of damage accumulation to predict the total life of test specimens. The predictions compare favorably with test data.

INTRODUCTION

The primary focus of the presented research is to demonstrate the feasibility of a probabilistic microstructural based fatigue modeling technique to predict the fatigue response of structures that include geometric details such as notches. The models predict the statistical parameters (mean and variance) of the fatigue strength of smooth bars of a titanium propulsion systems alloy at an R ratio of 0.1. (R ratio is defined as the minimum stress of a fatigue cycle divided by the maximum stress of a fatigue cycle.) The smooth bar model is then extended to model R ratio effect by changing only the applied loading. The material model remains unchanged. The R ratio model is then extended to model notch effects by changing only the stress concentration at the notch and the stressed surface area. Again, the material model remains unchanged. With the ability to separate the material model from the R ratio and notch models, the R ratio and notch effect become extrinsic to the material effects and true material fatigue behavior can be isolated and predicted.

The technology developed in the research will furnish a new design basis for structures, which will provide unique insight into the likely states of damage that can occur in a fleet of systems. Thus, the scatter in life and strength limiting conditions can be more accurately assessed early in the design phase or field operations for new and existing systems. In addition, new design concepts for damage avoidance and repair can be assessed in terms of their reliability for fleet applications. In all cases, the root cause of large scatter in various structural damage modes can be more fully understood; controls over production and inspection variables can then be imposed that contribute to the elimination of early, unanticipated structural failures.

FATIGUE MECHANISMS

The damage accumulation mechanisms operative in the crack nucleation and small crack growth stages depend on component fabrication related factors such as microstructure, texture, residual stresses and surface finish. The mechanisms also depend on the loading conditions such as amplitude, frequency, and mean stress along with environmental factors such as corrosion and temperature.

Ti-6Al-4V is valued due to the variety of microstructures and textures that can be produced by controlling the thermomechanical fabrication process. Two general classes of microstructures are used in gas turbine engines. One is the recrystallization annealed α-β structure which consist of relatively large α (hexagonal, close packed) platelets or spherical grains within a matrix of transformed β (body center cubic). Within the transformed beta

matrix are relatively small acicular α. The other microstructure is the annealed Widmanstatten or basketweave structure that consists of transformed β containing packets of acicular α with α at the prior β grain boundaries.

The wide variety of microstructures has also produced a wide variety of observed fatigue damage mechanics. In the α-β structure, Stubbington (1982) observed interface crack nucleation between the primary α and the β matrix at low stresses. They also observed interface cracking between the transformed β and the acicular α within the matrix. Slip band cracking of the primary α was observed as the stress was increased. Twinning, which is a deformation mode observed in the α phase of other titanium alloys is absent in Ti-6Al-4V. Benson *et al*. (1972) attributes this to the additional slip planes available in the α phase due to the aluminum as an alloy. Because of the slip characteristics of the α phase, preferred orientation due to forging has a significant affect on fatigue properties (Stubbington, 1982). Brown and Smith (1981) investigated the mechanisms of fatigue crack nucleation in α–β Ti-6Al-4V for R = 0 test. Nucleation was caused by slip in the α surface grains. The angle between the crack and the loading axis was approximately 45 degrees. Many of the surface cracks did not propagate into the neighboring grains. Cracks that caused final failure were associated with large (one to two grain) facets.

The alloy used in this investigation is a α–β Ti-6Al-4V (Peters *et al.*, 2000). The crack nucleation mechanisms modeled in this study are based on slip within the α grains and/or the transformed β matrix. It is assumed that the size and orientation of individual grains (or colonies) drive the nucleation mechanism as follows. Cracking occurs when the energy associated with dislocation density exceeds a critical level. The dislocation density depends on the resolved shear stress on the slip planes, which is a function of orientation, and the size of the grain (larger grains allow more dislocations to build up). Thus, large grains with favorable orientation will incur greater amounts of strain and cause cracking within the grain or at grain boundaries.

Several studies have investigated small crack behavior of “naturally” initiated cracks in smooth titanium specimens (Hall, 1997; Hines *et al*., 1999). Widely varying crack growth rates were observed for cracks with sizes on the order of the grain size. The crack growth rate changes from deceleration to acceleration upon the crack tip growing beyond the first or second α grain boundary. Very little crack growth rate deceleration is observed when the crack size is greater than 5 grains.

Irving and Beevers (1974) investigated the microstructural influences of fatigue crack growth in Ti-6Al-4V IMI 318. The near threshold long crack growth of several microstructures was investigated. Of particular interest is a α–β microstructure with α grains in a β matrix. The damage surface showed crystallographic crack growth in the α grains interrupted by the β matrix. The gross deviation out of the tensile crack plane indicated that a shear growth mode was involved in the α grains. The authors proposed that fracture of some of the α grains may take place ahead of the primary crack tip with intervening crack growth to connect the primary crack tip with the fractured grain. The intervening crack growth takes place in α grains and the β matrix. The β matrix appeared to fail by ductile rupture. Non-crystallographic crack growth (flat fracture surface) is observed when the size of the crack tip plastic zone exceeds the α grain size.

The small crack growth mechanisms modeled in this study are based the retardation mechanism caused by the microstructural obstacles (Hall, 1997). The obstacles appear to be the grain boundaries. The boundaries themselves are probably not fully responsible for the strength of the obstacle. The change in the medium from one grain to the next such as orientation differences from one α grain to the next or the change in crystalline structure from α grains to β matrix probably contributes to the strength of the obstacle. There seems to be an “inertia” that must be overcome for the crack tip to initiate damage in the grains in front of the crack tip. The obstacles cause radical variations in the crack growth rate of the small crack and sometimes permanent crack growth arrest. The wild fluctuations in the crack growth rate have an influence on the scatter in the fatigue life. It is the variation in crack growth arrest that can effect the scatter in the fatigue (infinite) strength.

The long crack mechanism may not be an important factor in the fatigue life of a high strength component with a naturally occurring

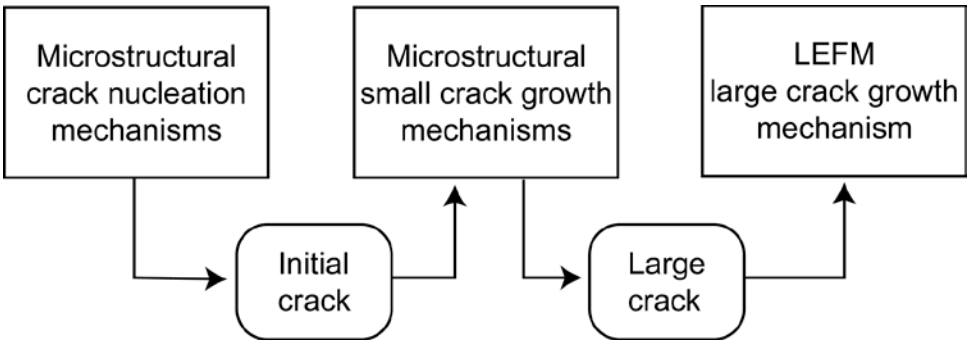

Figure 1: The three stages of the probabilistic microstructural fatigue algorithm.

crack. If loads are large enough to initiate and grow a crack through the small crack regime, the number of cycles needed to grow the crack through the long crack regime to final fracture could be insignificant. However, one aspect of the long crack regime -- long crack growth threshold -- can determine if the damage from an event will grow to failure. A long crack growth mechanism, based on linear elastic fracture mechanics (LEFM), is included in the overall fatigue damage simulation.

Based on the observed damage accumulation mechanism, the probabilistic microstructural fatigue algorithm will be modeled as three stages outlined in Figure 1. A cyclic plasticity mechanism causes dislocations to pile up against microstructural obstacles along slip bands within a grain. With each cycle of loading, more and more dislocations accumulate. If proper conditions exist, the energy associated with the dislocation accumulation can eventually exceed the energy needed to initiate a crack. At that point, an initial crack is formed. The crack is grown as a small crack by way of the interaction of dislocations generated at the crack tip with microstructural obstacles. The energy associated with these dislocations can cause the small crack to grow to a large crack if the proper conditions exist. At this point a large crack is formed and LEFM is used to growth the crack to final failure.

FATIGUE MODELS

Theoretical and semi-empirical models that relate the damage to the loading were developed based on those that have been proposed in the open literature. The models were modified to incorporate specific mechanisms and variables deemed important from the empirical observations.

CRACK NUCLEATION MODEL

Crack nucleation models based on cracking due to the build-up of dislocation density were incorporated into the probabilistic fatigue algorithm. Each surface grain is modeled as an individual homogeneous single crystal. Each grain has a unique size, orientation, applied stress and frictional strength. If the stress resolved on the slip plane exceeds the frictional stress, dislocations pile up at the grain boundary. If enough dislocations accumulate, the fracture energy of the grain is exceeded and the grain cracks. One such model that accounts for this mechanism is based on a model proposed by Tanaka and Mura (1981) for transgranular (or trans-colony) nucleation. This model was extended to account for grain orientation by Tryon and Cruse (1997) as

$$N_n = \frac{4GW_s}{\left(\frac{1}{M_s}\Delta\sigma - 2k\right)^2 \pi(1-\nu)d} \qquad (1)$$

where N_n is the number of cycles needed to grow a crack to the size of the grain, G is the shear modulus, W_s is the specific fracture energy per unit area, σ is the local applied normal stress, M_s is the grain orientation factor (reciprocal Schmid factor), k is the frictional stress which must be overcome to move dislocations, υ is Poisons ratio, and d is the grain diameter. Equation (1) is applicable to nucleation of cracks in either α or β grains. However, the parameters will be different depending on the phase of the grain.

SMALL CRACK GROWTH MODEL

The small crack growth model for Ti-6Al-4V is based on a recently developed model for single phase face center cubic microstructures (Tryon and Dey, 2001). The experimentally observable parameter that has been correlated to the varying small crack growth rate is the crack opening displacement (CTOD).

$$\frac{da}{dN} = C'\Delta\phi_t \qquad (2)$$

where *a* is the crack length, *N* is the number of cycles, *C'* and *n'* are empirical constants based on material testing. The CTOD, denoted by ϕ_t is measured at the location of crack extension for the previous cycle. The CTOD is a measure of the amount of damage associated with the crack tip. The larger the change in CTOD, the higher the crack growth rate. The direct proportionality of Eq (2) has been observed in small crack growth of aluminum, nickel and titanium alloys by Hicks and Brown (1984). Determining *C'* for small crack growth has been performed through direct microscopic observations or by using ΔK or ΔJ data.

Tanaka *et al*. (1986) developed a model to predict the CTOD based on the dislocations emitted from the crack tip and the blockage effect of the surrounding microstructure. Tanaka *et al.* (1992) used this model along with Monte Carlo simulation to predict the general behavior of small crack growth. The random variables included grain size, grain frictional stress, and an independent grain boundary strength. A two-parameter Weibull distribution was assumed for all of the random variables. They extended the model to include two-phase materials. Trends predicted by the model compared favorably with general trends observed in small crack growth behavior.

Tryon and Dey (2001) extended the approach used by Tanaka *et al*. (1986). The approach is outlined below for Mode II (sliding) crack growth. The solution for Mode I (tensile) crack growth is obtained through the simple transformations discussed latter.

Assume a crack has length *a* and the crack tip lies within a grain as shown in Figure 2. As load is applied, dislocations are emitted from the crack tip creating a slip band with dislocation density as represented by the length *w* in Figure 2. For low stress (where the applied stress is

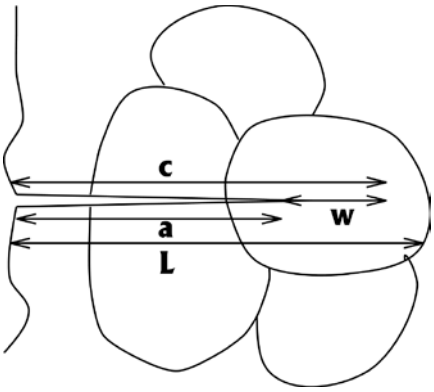

Figure 2: Crack surrounded by random microstructure with a slip band of width *w* extending from the crack tip.

greater than the stress needed to move dislocations) and the slip band tip far from the grain boundary (*c*<*L*). A condition called the *equilibrium slip band* exists.

The solution for the crack tip sliding displacement (CTSD) for the equilibrium slip band was obtained by Bilby *et al*. (1963). As the crack grows, the tip of the slip band will eventually be blocked at the grain boundary. This condition is called the *blocked slip band*. The solution for the CTSD for the blocked slip band was obtained by Taira *et al*. (1978).

As the crack grows, the stress intensity at the slip band tip, K_m increases. For the crack to overcome the grain boundary obstacle and propagate into the subsequent grain, K_m must exceed the critical microscopic stress intensity factor K_{mc} provided by the grain boundary. If as $a \to c$, K_m does not exceed K_{mc}, then the $\mathrm{CTSD} \to 0$ and the crack growth arrests. If K_m exceeds K_{mc}, the slip band tip propagates into the next grain and a condition called the *propagating slip band* exist. The solution for the CTSD for the propagated slip band was obtained by Tanaka *et al*. (1986).

Tanaka *et al*. (1992) solve for the case in which the slip band extends over several grains as shown in Figure 3 with the crack tip in the j^{th} grain and the slip band in the n^{th} grain. The Tanaka *et al*. (1992) model allows grain to grain variation in grain size and frictional stress. In Tryon and Dey (2001), the Tanaka *et al.* (1992) model is extended to include the variation in the microstress and the grain orientation by allowing grain to grain variation in the applied resolved

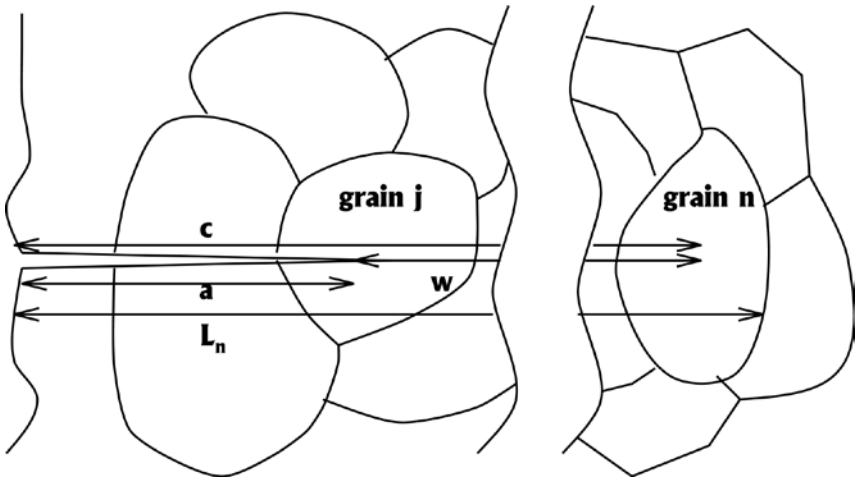

Figure 3: Crack surrounded by random microstructure with a slip band of width w extending from the crack tip over multiple grains.

shear stress τ. Consider a crack with the crack tip in the j^{th} grain and the slip band tip in the n^{th} grain. The equilibrium condition is

$$\tau^D + \tau^0 = 0$$

$$\tau^D = A\int_{-c}^{c} \frac{D(x')}{x - x'}dx'$$

$$A = \begin{cases} G/2\pi(1-\upsilon) & \text{for edge dislocations} \\ G/2\pi & \text{for screw dislocations} \end{cases} \quad (3)$$

$$\tau^0 = \begin{cases} \tau_j & x < a \\ \tau_j - k_j & a < x < L_j \\ \vdots & \vdots \\ \tau_n - k_n & L_{n-1} < x < c \end{cases}$$

where τ is the resolved applied shear stress, τ^D is the back stress caused by the dislocations, G is the shear modulus, a is the crack depth, c is the crack depth plus the slip band depth, L is the depth to the grain boundary, and k is the friction stress (which must be overcome to move dislocations) of the grain in which the crack tip and slip band lie. The dislocation density $D(x)$ is obtained by solving the singular integral of Eq. (3) using the inversion formula of Muskhelishvili (1977) for unbounded dislocation density at the crack tip.

For the propagated slip band, the size of the slip band zone can be found from

$$0 = \frac{\pi\tau_j}{2} - k_j \arccos\frac{a}{c} - \sum_{i=j+1}^{n} \left((\tau_{i-1} - k_{i-1}) - (\tau_i - k_i)\right)\arccos\left(\frac{L_{i-1}}{c}\right) \quad (4)$$

The CTSD φ_t is given by

$$\phi_t = +\frac{2k_j a}{\pi^2 A}\ln\frac{c}{a} + \sum_{i=j+1}^{n} \frac{(\tau_{i-1} - k_{i-1}) - (\tau_i - k_i)}{\pi^2 A} g(a; c, L_{i-1})$$

$$g(a;c,L) = L\ln\left|\frac{\sqrt{c^2 - L^2} + \sqrt{c^2 - a^2}}{\sqrt{c^2 - L^2} - \sqrt{c^2 - a^2}}\right| - a\ln\left|\frac{a\sqrt{c^2 - L^2} + L\sqrt{c^2 - a^2}}{a\sqrt{c^2 - L^2} - L\sqrt{c^2 - a^2}}\right| \quad (5)$$

For the blocked slip band, the size of the slip band zone is

$$w = L_n - a \quad (6)$$

The CTSD is given by

$$\phi_t = \frac{\beta\tau}{\pi A}\sqrt{c^2 - a^2} + \frac{2k_j a}{\pi^2 A}\ln\frac{c}{a} + \sum_{i=j+1}^{n}\frac{(\tau_{i-1} - k_{i-1}) - (\tau_i - k_i)}{\pi^2 A} g(a; c, L_{i-1})$$

$$\beta = 1 - \frac{2k_1}{\pi\tau_j}\arccos\frac{a}{c} - \sum_{i=j+1}^{n}\frac{2\left((\tau_{i-1} - k_{i-1}) - (\tau_i - k_i)\right)}{\pi\tau_j}\arccos\left(\frac{L_{i-1}}{c}\right) \quad (7)$$

The microscopic stress intensity factor is

$$K_m = \beta\tau\sqrt{\pi c} \quad (8)$$

The solution for Mode I loading is easily obtained through the following substitutions:

$$\tau \rightarrow \sigma$$

$$\text{CTSD} \rightarrow \text{CTOD}$$

where σ is the normal stress and CTOD is the crack tip opening displacement. The CTOD can now be predicted as a function of the microstructure that surrounds the small crack and then Eq. (2) can be used to predict the small crack growth rate. If there is randomness in the microstructure surrounding the small crack, the randomness can be directly related to the variation in the small crack growth rate.

LONG CRACK GROWTH MODEL

The long crack growth is modeled using the Paris law representation of a surface crack in a semi-infinite body subjected to a constant stress cycle. If the final crack size is much greater than the initial crack size,

$$N_g = \frac{a_i^{1-n/2}}{C\Delta\sigma^n\beta^n\left(\frac{n}{2} - 1\right)} \quad (9)$$

where, N_g is the number of cycles needed for the crack to grow to failure, a_i is the initial crack size at the start of the long crack growth phase, $\Delta\sigma$ is the global stress range, β is the geometry constant ($1.12\sqrt{\pi}$), and *C* and *n* are based on empirical material properties.

RANDOM VARIABLES

The important random variables for the Ti-6Al-4V alloy were identified through both existing empirical observations and the theoretical modeling considerations for each stage of damage accumulation. The statistical distributions, which serve as the quantitative measure of the random variables, were determined from theoretical considerations and empirical observations.

GRAIN SIZE

The grain size distribution was estimated from micrographs of the Ti-6Al-4V alloy (Peters *et al.*, 2000). The line intercept method was used to determine the alpha and transformed lamellar grain size. The micrographs of six specimens were used in the measurements. Measurements were taken along both axes. There was very little difference in the grain size between axes or between specimens. Measurements were made for 391 alpha grains. The average intercept length was $8.38\ \mu\text{m}$, the largest length was $30.4\ \mu\text{m}$ and the coefficient of variation (COV) was 0.59. Measurements were made for 208 transformed lamellar grains. The average intercept length was $7.44\ \mu\text{m}$, the largest length was $30.4\ \mu\text{m}$ and the COV was 0.71. The overall volume fraction was found to be 67%. The intercept distributions are shown in Figure 4 and Figure 5.

The crack nucleation model must consider the surface grain diameters formed by the surface "slicing" through the grains. This measurement will also be used to determine the distance between grain boundary obstacles during small crack growth. If it is assumed that the typical grain is spherical in nature, the line intercept method effectively slices each grain in a random manner such that

$$l = d_s\cos\left(\frac{\pi}{2}u\right)$$

where l is the intercept length, d_s is the diameter of the area of the intersection of the grain and the surface slice and u is the standard uniform random variable.

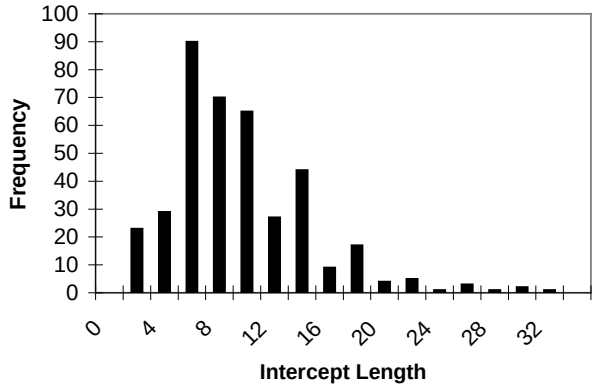

Figure 4: Distribution of alpha grain intercept lengths.

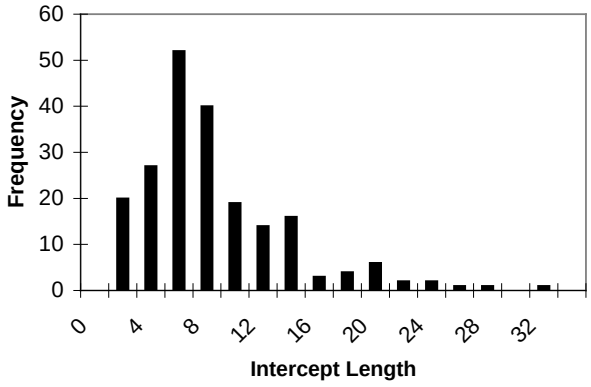

Figure 5: Distribution of transformed lamellar grain intercept lengths.

Monte Carlo simulation was used to evaluate the distribution of d_s by finding values of d_s that produce the measured mean and standard deviation of l. The mean of d_s for alpha grains was found to be $13.1\ \mu\text{m}$ and a standard deviation of $4.2\ \mu\text{m}$. The mean of d_s for transformed lamellar grains was found to be $11.8\ \mu\text{m}$ and a standard deviation of $5.5\ \mu\text{m}$.

GRAIN ORIENTATION

Models for randomly oriented α grains or β grains (colonies of α platelets within a β matrix) were not available in the open literature. Therefore, appropriate models had to be developed.

Slip orientation for a primary α grain

Tryon and Cruse (1997) developed a method to determine the statistical distribution of orientation factor (Schmid or Taylor) for randomly orientated grains using the orientation factor defined within the stereographic triangle for face center cubic (FCC) structures. The studies on the orientation factor for α (HCP) titanium grains appear to have been very limited. However, Tan *et al.,*(1997) determined the Schmid factor throughout the stereographic triangle for the 5 most active slip systems and 3 most active twin systems for high purity HCP titanium. Fundenberger *et al.,* (1997) showed that for small strains, the basal and pyramidal slip along the $< a >$ Burgers vector are most active in ($\alpha + \beta$) Ti-6Al-4V. (Twinning does not seem to be active in Ti-6Al-4V.) Assuming these slip systems are equally active, the distribution of the reciprocal Schmid factor can be determined in the same manner as Tryon (2000). Figure 6 shows the reciprocal Schmid factor distribution for Ti-6Al-4V.

Slip orientation for a colony of α platelets

Bache *et al.* (1998) studied large (essentially single) colonies of a titanium alloy with aligned α laths in a β matrix. They showed that colony orientation determines the kinetics of crack development. Early fatigue damage accumulation involved cracking along slip band parallel to the α/β interface. In an earlier study, Chen *et al.* (1981) examined yield characteristics of single colonies of a titanium alloy with aligned α platelets in a β matrix. They found that the initial micro yielding took place on slip planes in the α phase. The easy slip system was parallel to the α/β interface and was governed by Schmid's law. They attribute this to the long slip length available in the plane of the plate. The activation of this slip system was dependent on the angle of the platelet with the direction of the applied loading. For a polycrystal with millions of colonies, there will be many colonies oriented for easy slip and thus easy slip will govern crack initiation at the low stress level associated with long life fatigue.

Each platelet will have an easy slip plane parallel to the α/β interface (in the plane of the plate). However, the slip direction on the slip plane is assumed to be random. Because a

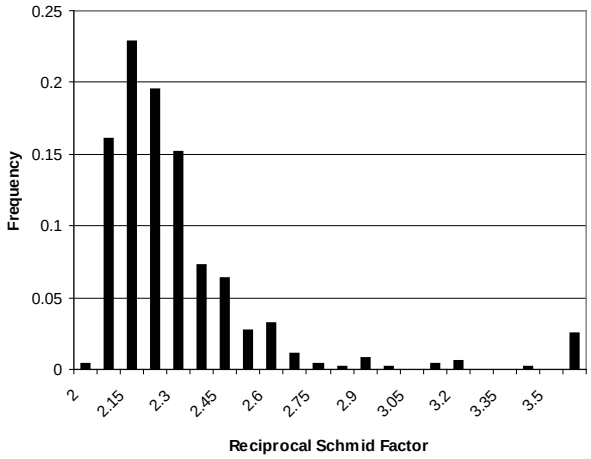

Figure 6: Probability density function of the reciprocal Schmid factor for HCP structures.

colony is composed of several α platelets, it is assumed that at least one of the α platelets will have a favorable slip direction. This will be the controlling α platelet. Therefore, the slip direction of the controlling α platelet will have a slip direction angle λ that is the complement of the slip plane angle ζ. The statistical distribution of the Schmid factor for a colony of α platelets is determined using procedure outlined in Tryon (2000). The results of the analysis are shown in Figure 7.

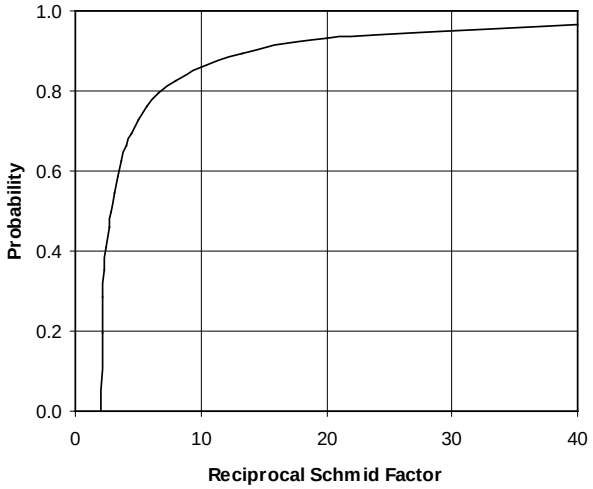

Figure 7: Cumulative distribution function (cdf) of the reciprocal Schmid factor for a colony of α platelets.

FATIGUE PREDICTION ALGORITHM

A numerical algorithm based on the microstructural models and random variables presented previously were developed to simulate the overall life of an ensemble of simple test specimens. The algorithm used a nested approach. The damage accumulation started on the smallest scale and grew through the various stages of damage accumulation and crack growth.

For demonstrating the algorithm, consider the fatigue analysis of a smooth round bar test specimen subjected to constant amplitude axial loading. The input to the algorithm includes:

Component level variables

1. number of bars to be tested
2. applied load
3. gage section surface area
4. volume fraction of alpha phase

Macrostructural material variables

1. shear modulus
2. Poisson's ratio
3. specific fracture energy
4. long crack Paris law exponent
5. long crack Paris law coefficient (random variable)
6. short crack Paris law coefficient

Microstructural material variables

1. grain diameter (random variable)
2. grain orientation (random variable)
3. frictional strength i.e., stress needed to move dislocations (random variable)
4. microstress factor i.e., factor that is multiplied by the applied stress to determine the stress at the level of the grain size (random variable)
5. grain boundary stress intensity factor i.e., stress intensity factor that must be exceeded to overcome the grain boundary strength.

The basic flow of the algorithm is outlined as follows:

1. A bar is chosen and the grains of the bar are generated. Each grain has a distinct size,

orientation, frictional strength and microstress.
2. A crack is nucleated in a surface grain and the cycles to initiation are found .
3. The crack then grows through the microstructure via small and then long crack growth models.
4. Another grain is chosen and Steps 2 and 3 are repeated.
5. Step 4 is repeated multiple times until all surface grains are considered. However, step 3 is not repeated for all of the surface grains. A method of choosing only the grains that initiate a crack that is likely to lead to failure is employed.
6. The life of the component is set equal to the minimum life of all of the cracks.
7. The next bar is generated and the process is repeated.

The details of the simulation can be found in Tryon and Dey (2001).

RESULTS OBTAINED

A FORTRAN software program was created to predict the fatigue response. A Monte Carlo based modeling algorithm was developed using the models and random variables outlined above. The Monte Carlo technique is used to generate the random microstructure and the damage accumulation models were used to simulate the fatigue damage growing through the microstructure.

Table 1 shows the values of the random variables used for the algorithm. Most of the values in Table 1 were determined based on data in the open literature outlined previously. Parameters values that were not specifically available include the CTOD Law Coefficient, *C',* and the specific fracture energy, W_S. The CTOD Law Coefficient was determined from the slope of short crack growth da/dn versus ΔK data from an unpublished U. S. Air Force sponsored smooth bar short crack test. However, due to the large scatter in the measured slopes, it was difficult to determine a representative value. Therefore, *C'* was bounded by examining the experimental data and *C'* and W_S were determined by fitting the mean simulated fatigue lives for the various stages of fatigue to the observed mean fatigue lives of the short crack test with a normalized maximum stress (maximum applied stress divided by the yield strength) of 0.635 and R ratio of 0.1. These test data were used because transitions from crack nucleation to short crack growth to long crack growth were observed using intermittent surface replications. The value of *C'* was 0.0075. The value of W_S was 2000 lbs/in. The grain boundary stress intensity factor (SIF) K_C, was based on intrinsic threshold SIF data by Ritchie *et al.* (1999).

SMOOTH BAR RESULTS

Table 1: Parameter values used for the analysis

Variable	Description	Distribution	Average	COV
C	Paris Law Coefficient	Lognormal	6.58E-11	0.3
C'	CTOD Law Coefficient	Deterministic	0.0075	N/A
d_α	α grain diameter	Lognormal	0.516 mils	0.32
d_β	β grain diameter	Lognormal	0.350 mils	0.47
G	Bulk shear modulus	Deterministic	7.16 Msi	N/A
k_α	α frictional strength	Weibull	110 ksi	0.10
k_β	β frictional strength	Weibull	100 ksi	0.10
K_C	Grain boundary SIF	Deterministic	2 ksi$\sqrt{}$in	N/A
M_α	α orientation factor	See Figure 6	2.35	3.83
M_β	β orientation factor	See Figure 7	2.86	3.15
n	Paris law exponent	Deterministic	3.96	N/A
W_S	Specific fracture energy	Deterministic	2000 lbs/in	N/A
σ	Micro-stress	Normal	Applied stress	0.3
υ	Poisson's ratio	Deterministic	3.4	N/A
A	Gage section area	Deterministic	0.471 in^2	N/A

The model successfully simulated the general fatigue behavior observed in the test data. The predicted results are compared with actual test results from the load controlled tests (R=0.1) in Figure 8. The stress level in the figure is normalized by the yield stress. The simulation predicts that the majority of life is spent in the crack nucleation phase for all stress levels and the percentage of life spent in crack nucleation increases with decreasing stress. These predictions were observed during the test. The test produced suspensions at stress values of about 0.6 and below. The model predicts increasing suspensions as the stress is lowered below 0.6. The model also predicted a suspension at a stress of 0.64 that was not observed during the testing. However, it is possible that a suspensions could occur at 0.64 if more specimens were tested.

By closely monitoring the simulation algorithm, a better understanding can be gained of the phenomenon of increasing scatter with decreasing load. The model predicts that cracks nucleate in grains depending on the orientation, size, etc. The crack grows to failure if it can overcome the surrounding microstructural obstacles. At low stress, most grains do not have the proper orientation and size to nucleate a crack. Those grains that are successful in nucleating the crack may not overcome the surrounding microstructure. These grains can be considered to have “infinite life”. Only a few grains will have the proper orientation, size and surrounding microstructure to nucleate and grow a crack. These grains can be considered to have “finite life”. However, at high stress, more grains will nucleate cracks. At high stress, the crack has a better chance of overcoming the surrounding microstructure. Therefore, at high stress, more grains have “finite life”.

The life of the specimen is equal to the crack that nucleates and grows the quickest i.e., the grain with the lowest finite life. Therefore, the fatigue life is governed by an extreme value problem. Each specimen can be thought of as a pool of grains with finite life. The lowest life grain of that pool governs the fatigue life of the specimen. At high stress, there are more grains with finite life and thus a large pool from which to choose. At low stress, there are fewer grains with finite life and thus a small pool from which to choose. If we choose the extreme life from 15 pools with many grains (15 bars tested at a stress of 0.7) there will be less scatter among the lives than if we choose the extreme life from 15 pools with few grains (15 bars tested at a stress of 0.6) This is typical of extreme value problems.

The simulation predicted that several grains

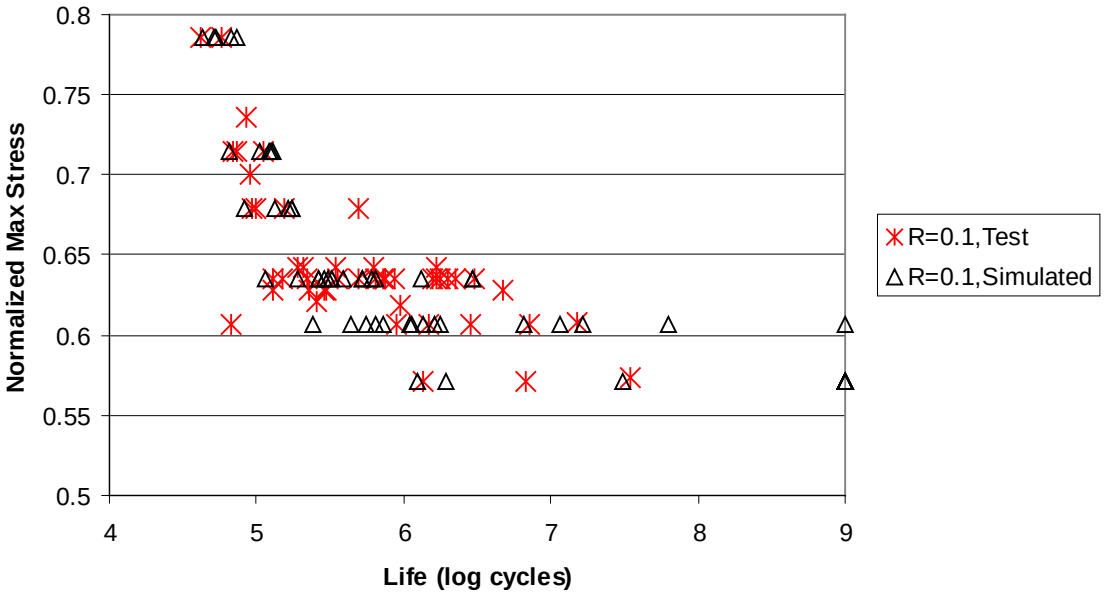

Figure 8: Comparison of simulation predictions with actual test data for R = 0.1.

nucleated cracks at high stress (as many as 20 grains out of the 2 million or so surface grains). The fatigue test indicated that only one crack was observed to nucleate, even at high stress. It may appear that the simulated fatigue response violates this observation. However, these grains were not surrounded by a sympathetic microstructure and were unable to grow. During the laboratory test, it would be very difficult to observe these cracks due to their extremely small size and relative rarity. In addition, the specimen surfaces were etched to elucidate the microstructure via plastic replication. Differentiating the sub-grain cracks from other microstructural features would be almost impossible using replication.

The other R ratio tests were simulated using the data in Table 1 and by inputting the same maximum and minimum stresses applied during the R ratio test. Figure 9 shows the comparison between the simulated and actual test data. In general, the model appears to successfully simulate the R ratio effect; however, no attempt was made to correlate the model for R ratio.

For the R=0.5 test, the model successfully predicted the mean and scatter of the fatigue lives of the various stresses with the following exceptions. The model did not predict the mean life at the highest stress of 0.93. This stress is near the yield strength and as one might expect, other failure mechanisms may be involved. In addition, the model predicted no failures below a stress of 0.75; however, test failures were observed at a stress of 0.71. Test suspensions were found to occur at a stress of 0.68 whereas the model predicted suspensions at 0.75. Based on these results, further investigation of the R=0.5 test at low stress is warranted.

For the R=-1 test, the model predicted the mean and scatter of the fatigue lives of the various stresses except for the threshold behavior. The model predicted no failures below a stress of 0.48. Although test suspensions were observed at similar stresses, failures were observed at stresses as low as 0.39. Based on these results, further investigation of the R=-1 test is warranted. However, in general, the fatigue algorithm successfully captured the overall R ratio behavior.

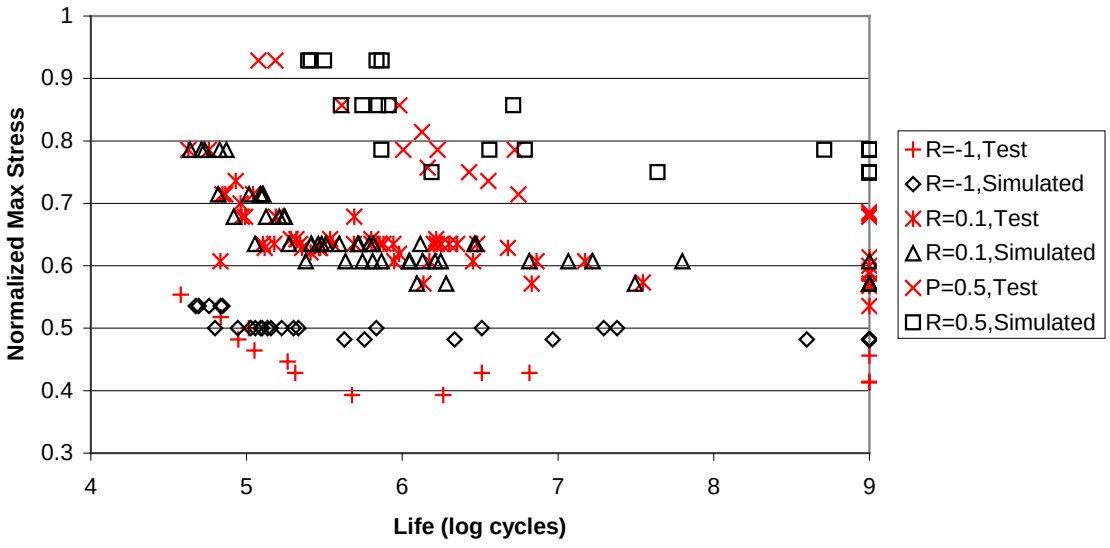

Figure 9: Comparison of simulation predictions with actual test data for various R ratios.

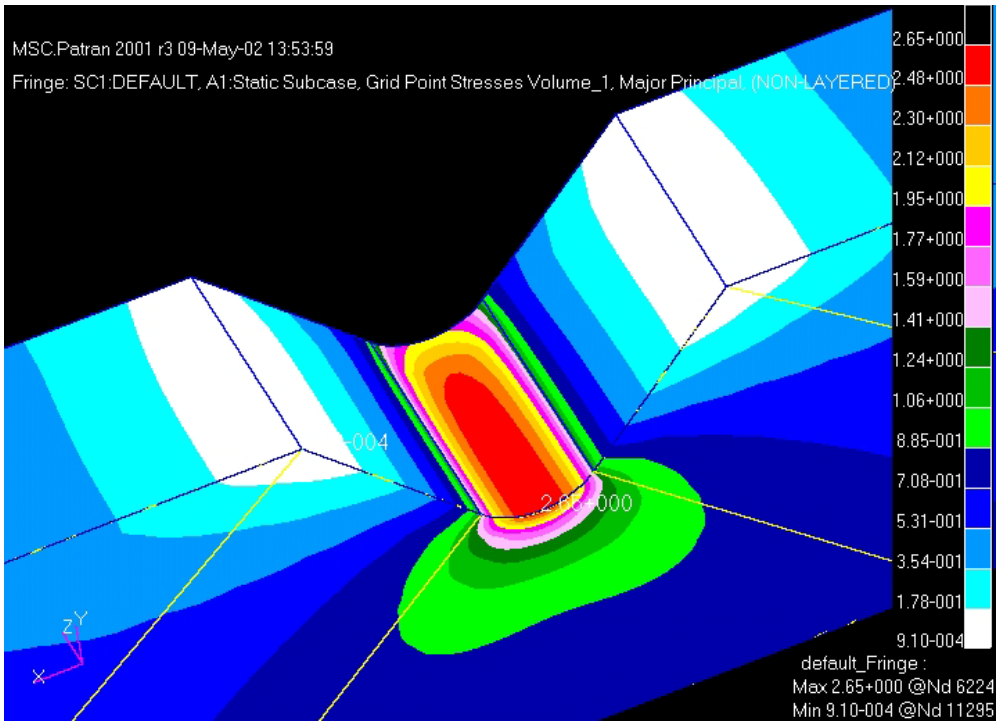

Figure 10: FEM results of maximum principal stress at notch root.

NOTCHED BAR RESULTS

The U. S. Air Force sponsored other unpublished research in which fatigue tests were performed on standard notched Ti-6Al-4V specimen with a notch radius of 0.021 inches. For the current research, a notched specimen finite element model (FEM) representing the double notch specimen was created. The FEM was used to determine the stress concentration (K_T) at the notch root and the surface area corresponding to the K_T . The results of the FEM are shown in Figure 10 with a predicted K_T of 2.65.

One hundred twenty surface elements had a K_T above one (1). It was assumed that element with stress concentrations below one would not have stresses of sufficient magnitude to cause fatigue failures because the applied stresses in the of notched specimen tests were well below the fatigue limit of smooth specimens. The stress concentration and area of each of the 120 surface elements was cataloged. Because the model (Figure 10) represents one quarter of the double notched specimen, the area of each surface element was multiplied by four to properly represent the stressed surface area for the entire double notched specimen.

A stress gradient through the thickness along the center line of the model (y-direction in Figure 10) is shown in Figure 11. A polynomial equation approximating the stress gradient was determined and is shown in Figure 11 along with the R-squared goodness of fit parameter. It is assumed that a crack growing from any of the 120 surface elements will experience the same

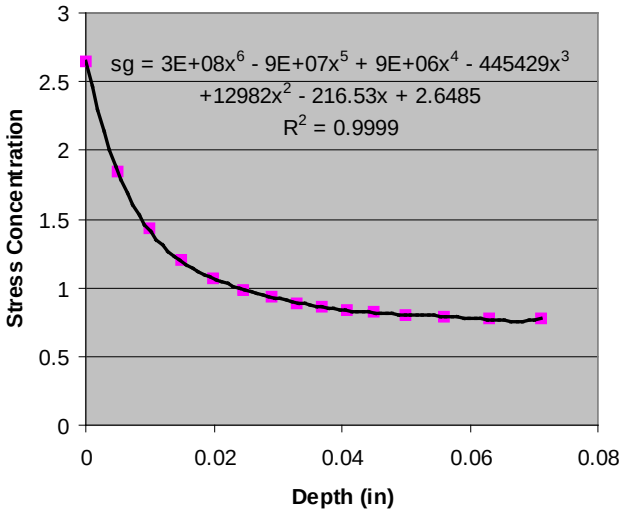

Figure 11: Stress concentration gradient through specimen thickness.

stress gradient weighted by the surface element K_T divided by the K_T at the center line. This is a reasonable assumption because the iso-stress lines are concentric in the y-direction as shown in Figure 10. Thus,

$$sg_n = sg \frac{K_{Tn}}{2.6486} \quad (10)$$

where sg_n is the stress gradient for any surface element *n*, sg is the stress gradient at the center line as shown in Figure 11 and K_{Tn} is the stress concentration of the n^{th} surface element.

The Figure 11 results show a decrease in stress as a function of the distance away from the centerline. Assuming the average grain diameter of Ti-6Al-4V is 0.0005 inches, the figure indicates that there is considerable decrease in the stress over relatively few grains. Based on this, it can be concluded that the stress concentration is on the microstructural scale. In the short crack regime (approximately ten grain diameters), the stress drops 30 percent from the surface value.

A strategy was defined to predict the notch effect on fatigue as presented below.

1. The elemental stress is determined for each element on the surface of the notch.
2. All elements with stresses below the user-specified fatigue limit are removed from consideration.
3. The surface area of each element is determined.
4. It is assumed that a crack grows perpendicular to the applied loading. Thus, the stress from the center of each surface element along a line perpendicular to the applied loading is determined. (see Figure 11)
5. An equation is fit to the stress as a function of distance from the surface (See Eq. (10)).
6. The crack nucleation algorithm of the probabilistic microstructural fatigue model remains essentially unchanged. The surface stress is used to determine crack nucleation for all grains on each surface element.
7. The short crack growth software algorithm is revised to allow the applied stress to vary along the crack path using the equation determined in Step 5.
8. The long crack growth software algorithm is revised to allow the applied stress to vary along the crack path using the equation determined in Step 5.

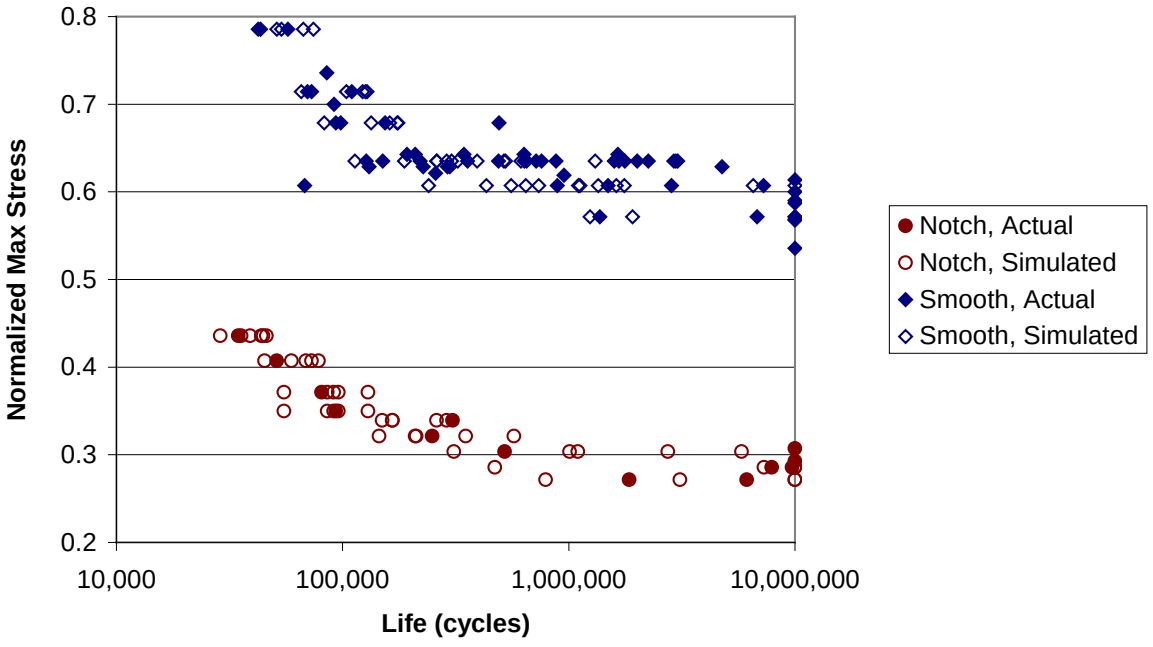

Figure 12: Comparison of notched and smooth test data with simulated data for R = 0.1.

To evaluate the efficacy of the notch modeling methodology, the fatigue tests on the standard notch Ti-6Al-4V specimens were simulated. The microstructural material properties are the same as shown in Table 1. The objective of this evaluation was to determine if the probabilistic microstructural fatigue model can predict the notch effect as an extrinsic effect and not a material model effect.

For each actual test stress level, five notched specimens were simulated using the fatigue algorithm. Figure 12 shows the comparison of notched test data with simulated data for R = 0.1. The figure shows that the simulated data compares well with the actual test data for all the stress level tests. The predicted scatter from the simulation model is similar to the scatter in the test data. The actual tests resulted in suspension at 10e7 cycles at an applied stress of 0.31. Similarly, the simulated test data predicted suspensions at 0.30. Figure 12 also shows the comparison of the smooth and notched specimen test of the Ti-6Al-4V alloy. The simulation-based model appears to appropriately predict the degradation in fatigue properties from the smooth specimen to the notched specimen.

Figure 13 shows the comparison of notched test data with simulated data for R = -1. Figure 13 also shows the results for the smooth specimen test of the Ti-6Al-4V alloy. As discussed previously, the smooth R = -1 simulation successfully predicted the mean stress effect except at low stress (below 0.47). (The fatigue failure mechanism may be different at this stress level. The mechanisms used in the probabilistic microstructural model were observed at a stress of 0.64.) Similarly, the simulated notch predictions appear to compare well with the test data except at low stress (below 0.21). Notched test specimen failures were observed at an applied stress as low as 0.2, while the simulation did not predict failures below 0.22. The simulated data predicted scatter appears to be similar to the scatter in the test data. Although the simulated data may appear to indicate a higher scatter (i.e., longer lives than the test data below a stress of 0.24), test suspension at 10e7 cycles were observed at a stress of 0.24. Thus, there is also large scatter in the test data at 0.24. The simulation predicted suspensions at a stress of 0.24.

One must be mindful that the material properties inputs to the simulation model are based on R =

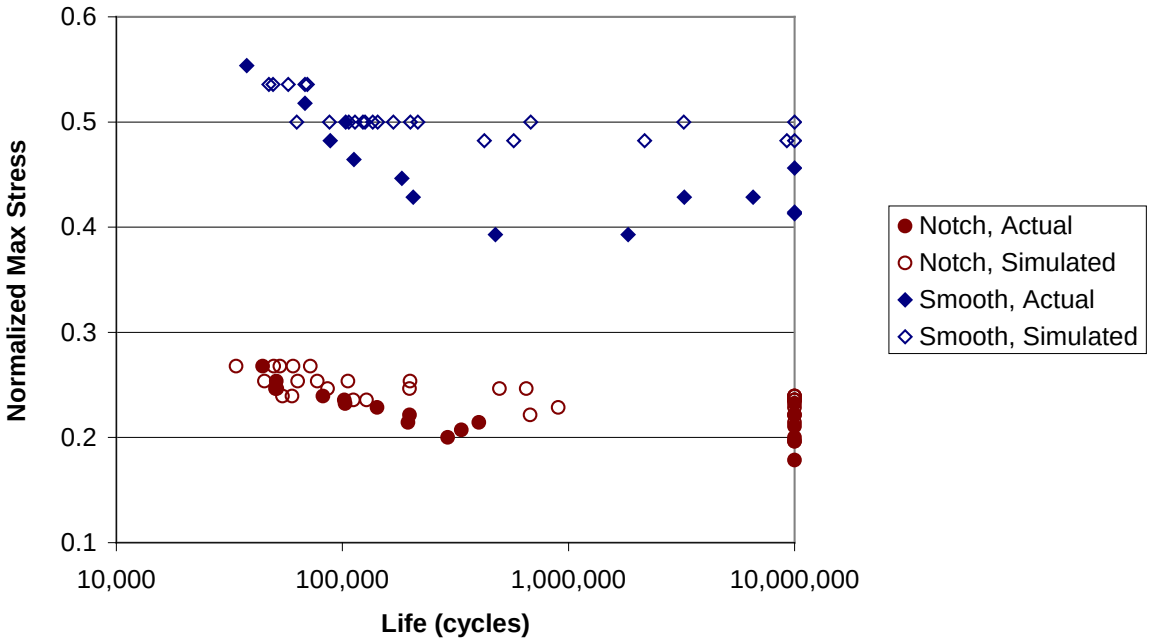

Figure 13: Comparison of notched and smooth test data with simulated data for R = -1.

0.1 smooth bar material data. Therefore, the model is simulating the combination of the notch effects *and* mean stress effects. Since the apparent discrepancies in the notch model at R= -1 are similar to the discrepancies in the smooth model at R = -1, the probabilistic microstructural fatigue model appears to be accurately capturing the notch effect.

Figure 14 shows the comparison of notched test data with simulated data for R = 0.5. Figure 14 also shows the results for the smooth specimen test. As discussed previously, the smooth R = 0.5 data simulation accurately predicted the mean stress effect except at high stress (above 0.86). (The fatigue failure mechanism may be different at this stress level. The mechanisms used in the probabilistic microstructural model were observed at a stress of 0.64.) Similarly, the simulated notch predictions appear to compare well with the test data except at high stress (above 0.44) where failures occurred earlier than predicted. No notched specimen failures were observed below an applies stress of 0.39. The simulation also predicted no failures below 0.39. The simulation predicted scatter is similar to the scatter in the test data. Test suspensions at 10e7 cycles were predicted at an applied stress of 0.41 This is in reasonable agreement with the test data for the limited number of specimens tested considering a test failure at 3.3e6 cycles at an applied stress of 0.39.

Similar to the R = -1 simulation, the material properties inputs to the R = 0.5 simulation are the same as the R = 0.1 smooth bar simulation. Therefore, the model is simulating the combination of the notch effects *and* mean stress effects. It appears that the discrepancies in the notch model at R= 0.5 are similar to the discrepancies in the smooth model at R = 0.5 and thus, the simulation appears to be appropriately predicting the notch effect.

CONCLUSION

The probabilistic microstructural fatigue model appears to be appropriately predicting the R ratio and notch effects. The material properties used in the models were unchanged from those used in the smooth bar R = 0.1 model. The R ratio was modeled based solely on the applied maximum and minimum stresses. The notch was modeled based solely on the stressed volume of material determined from the finite element model. Thus, extrinsic parameters such as geometry and loading determine the effect of the notch. No adjustments need to be made to the material properties. In general, the proposed probabilistic microstructural fatigue simulation

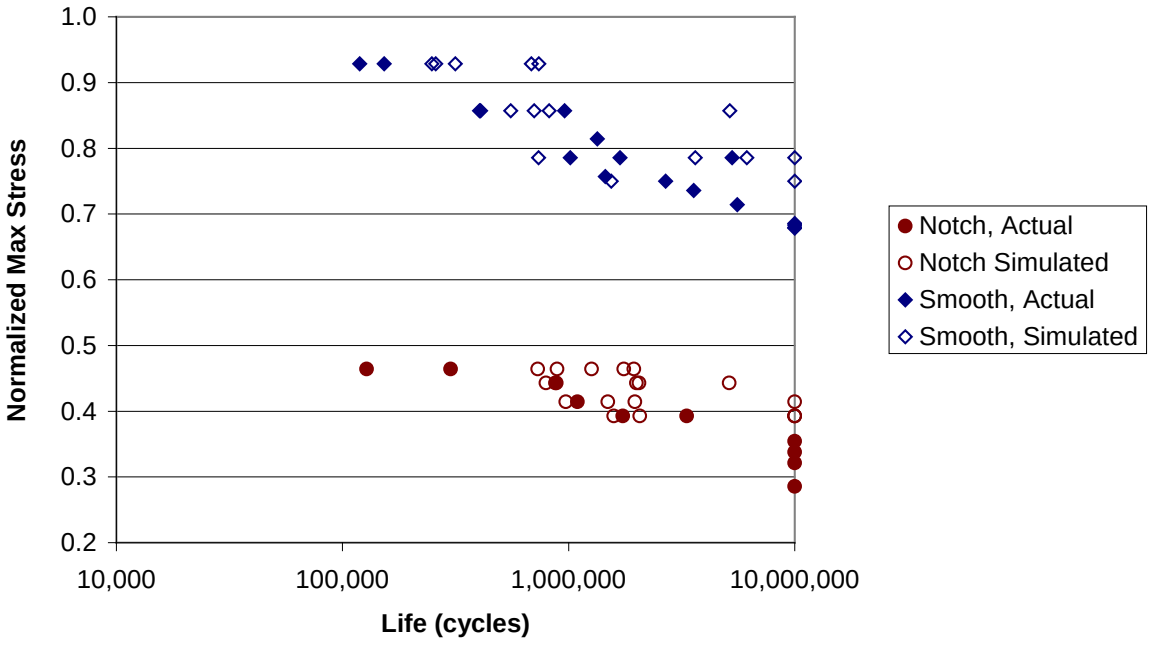

Figure 14: Comparison of notched and smooth test data with simulated data for R = 0.5.

should be able to predict the response of a component with arbitrary geometry and arbitrary loading.

ACKNOWLEDGMENTS

The research was supported by U. S. Air Force contracts F33615-00-C-5209 and F33615-01-C-5228. The authors thank Drs. J. Calcaterra, J. Jira, R. Morrissey and A. Rosenberger for their support.

REFERENCES

1. Bache, M. R., Evans, W. J., Randle, V., Wilson, R. J., (1998) “Characterization of mechanical anisotropy in titanium alloys.” Mat. Sci. Engrg., A257, pp. 139-144.
2. Bilby, B. A., Cottrell, A. H., Swinden, K. H., (1963) “The Spread of Plastic Yield from a Notch,” Proc. Roy. Soc., Vol. A272, pp. 304-314.
3. Hall, J. A., (1997) “Fatigue crack initiation in alpha-beta titanium alloys,” Int. J. Fatigue, Vol. 19, Supp. No. 1, pp. S23-S37.
4. Hicks, M. A., Brown, C. W., (1984) “A comparison of short crack growth behavior in engineering alloys,” *Fatigue 84*, Engineering Materials Advisory Services Ltd., England, pp. 1337-1347.
5. Hines, J. A., Peters, J. O., Lutjering, G., (1999) “Microcrack propagation in the LCF- and HCF- regime in Ti-6Al-4V.” 9th World Conf. On Titanium Alloys, St. Petersburg, Russia.
6. Muskhelishvili, N. I.,(1977) *Singular Integral Equations*, Noordhoff International.
7. Peters, J. O., Roder, O., Boyce, B. L., Thompson, A. W., Ritchie, R. O., (2000) “Role of foreign object damage on the threshold for high cycle fatigue in Ti-6Al-4V.” Report # UCB/R/99/A1166.
8. Ritchie, R. O., Davidson, D. L., Boyce, B. L., Roder, O., (1999) “High cycle fatigue of Ti-6Al-4V,” Fat. Frac. Eng. Mat. Str., Vol. 22.
9. Stubbington, C. A., (1982) “Metallurgical aspects of fatigue and fracture in titanium alloys.” Titanium and Titanium Alloys, ASM, 140-158.
10. Tan, X., Gu, H., Laird, C., Munroe, N. D. H., (1998) “Cyclic deformation behavior of high-purity titanium single crystals: Part I. Orientation dependence of stress-strain response,” *Metall. Mater. Trans.*, Vol. 29A, pp. 507-512.
11. Tanaka, K., Mura, T., (1981) “A dislocation model for fatigue crack initiation.” *ASME J. Appl. Mech*. Vol. 48, 97-103.
12. Tanaka, K., Akiniwa, Y., Nakia, Y., Wei, R. P., (1986) “Modeling of Small Fatigue Crack Growth Interacting with Grain Boundary,” Engng. Frac. Mechs., Vol. 24, No. 6, pp. 803-819.
13. Tanaka K., Kinefuchi, M., and Yokomaku, T., (1992) “Modelling of Statistical Characteristics of the Propagation of Small Fatigue Cracks,” *Short Fatigue Cracks*, Eds. Miller, K. J., and de los Rios, E. R., ESIS 13, Mechanical Engineering Publications, London, pp. 351-368.
14. Tanaka, T., Kosugi, M., (1988) “Crystallographic Study of the Fatigue Crack Nucleation Mechanism in Pure Iron,” *Basic Questions in Fatigue*, Vol. 1, ASTM STP 924, pp. 98-119.
15. Taira, S., Tanaka, K., Nakai, Y., (1978) “A Model of Crack Tip Slip Band Blocked by Grain Boundary,” Mech. Res. Comm., Vol. 5, No. 6, pp. 375-381.
16. Tryon, R. G., Cruse, T. A., (1997) “Probabilistic mesomechanical fatigue crack nucleation model,” J. Engr. Mater. Tech., Vol. 119, pp. 65-70.
17. Tryon, R. G., (2000) “Probabilistic Orientation Model for TiAl Ordered Intermetallic.” ASCE Specialty Conference on Probabilistic Mechanics and Structural Reliability, July 24-26 Notre Dame, IN, paper PMC2000-154.
18. Tryon, R. G., Dey, A., (2001) “Reliability-Based Computational Model for Material Development and Structural Design,” International Journal of Materials and Product Technology, Vol. 16, No. 4/5, pp. 333-357.